Revisiting the CooJ family, a potential chaperone for nickel delivery to [NiFe]-carbon monoxide dehydrogenase

Elisabeth Darrouzet, Clara Rinaldi, Barbara Zambelli, Stefano Ciurli, Christine Cavazza

Revisiting the CooJ family, a potential chaperone for nickel delivery to [NiFe]-carbon monoxide dehydrogenase

Elisabeth Darrouzet[a], Clara Rinaldi[a], Barbara Zambelli[b], Stefano Ciurli[b], Christine Cavazza[a,*]

[a] University of Grenoble Alpes, CEA, CNRS, IRIG, CBM, F-38000 Grenoble, France
[b] Laboratory of Bioinorganic Chemistry, Department of Pharmacy and Biotechnology, University of Bologna, Via Giuseppe Fanin 40, I-40127 Bologna, Italy

*To whom correspondence should be addressed: christine.cavazza@cea.fr

ABSTRACT

Nickel insertion into nickel-dependent carbon monoxide dehydrogenase (CODH) represents a key step in the enzyme activation. This is the last step of the biosynthesis of the active site, which contains an atypical heteronuclear $NiFe_4S_4$ cluster known as the C-cluster. The enzyme maturation is performed by three accessory proteins, namely CooC, CooT and CooJ. Among them, CooJ from *Rhodospirillum rubrum* is a histidine-rich protein containing two distinct and spatially separated Ni(II)-binding sites: a N-terminal high affinity site (HAS) and a histidine tail at the C-terminus. In 46 CooJ homologues, the HAS motif was found to be strictly conserved with a H(W/F)XXHXXXH sequence. Here, a proteome database search identified at least 150 CooJ homologues and revealed distinct motifs for HAS, featuring 2, 3 or 4 histidines. The purification and biophysical characterization of three representative members of this protein family showed that they are all homodimers able to bind Ni(II) ions *via* one or two independent binding sites. Initially thought to be present only in *R. rubrum*, this study strongly suggests that CooJ could play a significant role in CODH maturation or in nickel homeostasis.

KEYWORDS

Nickel chaperone, carbon monoxide dehydrogenase, enzyme maturation, histidine-rich protein, proteome databases, nickel trafficking.

1 Introduction

Nickel-dependent carbon monoxide dehydrogenase (CODH) catalyzes the reversible oxidation of CO to CO_2. Depending on the metabolic context, the enzyme occurs in a monofunctional or bifunctional form. In the latter case, CODH is coupled to acetyl coenzyme A (acetyl-CoA) synthase (ACS) to form the CODH/ACS complex in anaerobic bacteria or the acetyl-CoA decarbonyl/synthase (ACDS) complex in archaea [1]. This enzyme complex catalyzes the synthesis of acetyl-CoA from coenzyme A condensed with CO, derived from CO_2 reduction. On the other hand, monofunctional CODH are often described as CO-oxidizing enzymes involved in the energy metabolism of carboxydotrophs, although their function has not been clearly identified in some bacteria. For example, in *C. hydrogenoformans*, CODH-IV would play a role in defense against oxidative stress [2]. The active site of CODH, known as the C-cluster, contains a $NiFe_3S_4$ cluster connected to a mononuclear Fe (Fe1) through a linking sulfide [3] (Scheme 1). The protein provides four cysteine ligands to bind the cluster (three for the iron atoms and one for the nickel atom), in addition to a cysteine and a histidine to coordinate Fe1. Given the complexity of this multi-metallic active site, it is not surprising that its assembly and insertion into the protein requires a specific maturation machinery. The maturation pathway of CODH is a multistep process involving two consecutive events. The biosynthesis process of the C-cluster starts with the insertion of Fe and S atoms to form a Fe_4S_4 cluster, likely performed by the classical iron-sulfur cluster (ISC)/sulfur mobilization (SUF) machineries responsible for FeS cluster biogenesis [4], as shown by the production of a fully FeS-loaded CODH produced in *E. coli* [5]. The following step is the insertion of the Ni atom, known as a key step in the enzyme activation, carried out by the concerted action of three nickel-binding proteins: the nickel-dependent ATPase CooC [6], [7] and two additional nickel chaperones CooT and CooJ. Although CooC is described as the major player in CODH maturation, CooJ [8], [9],[10] and CooT [11] are nevertheless relevant for *in vivo* nickel delivery to CODH in *Rhodospirillum rubrum* [12]. In this carboxydotrophic bacterium, CODH is encoded by the c*ooFSCTJ* operon, which in turn is regulated by the CO-sensing transcriptional activator CooA. [1] The *cooFSCTJ* operon contains five genes encoding the ferredoxin CooF (the physiological partner of the enzyme), the monofunctional CODH CooS and the three nickel proteins CooC, CooT and CooJ. Until a few years ago, CooJ and CooT from *R. rubrum* were described as the only representatives of their family [12]. However, recent phylogenetic analyses highlighted the existence of at least 111 CooT homologues in anaerobic archaea and bacteria (co-occuring with CODH and CooC in most of the cases) [11] and at least 46 CooJ homologues in bacteria [8].

These recent observations suggest different maturation pathways for CODH with the requirement of CooC alone, or in association with CooT and/or CooJ.

CooJ from *Rhodospirillum rubrum* (*Rr*CooJ) is a 12.5 kDa protein containing a disordered C-terminal domain with 16 histidines and 2 cysteines in the final 34 amino acids. When *Rr*CooJ was purified directly from *R. rubrum* cultures, the protein co-eluted with CODH, and was able to bind 4 Ni(II) per monomer with an affinity in the micromolar range [9]. The histidine-rich region (HRR) of *Rr*CooJ is partially dispensable to fulfill its physiological function, suggesting a non-essential role of this histidine tail in CODH maturation. Recently, the recombinant *Rr*CooJ protein overproduced in *E. coli* was thoroughly characterized: the protein is a homodimer formed by an anti-parallel coiled coil with two independent and highly flexible HRR arranged head-to-tail [8]. As expected by the presence of two intrinsically disordered His tails, *Rr*CooJ has a strong tendency to form oligomers through interactions with Ni(II)[10]. Indeed, in the presence of Ni(II), *Rr*CooJ exists as an equilibrium of oligomeric states in solution, while the apo-protein forms a stable dimer. Two phenomena were observed upon nickel addition. First, Ni(II)-binding directly impacts the secondary structure content of the protein, with a gain in α-helices related to a higher stability. Second, nickel induces a dynamic and reversible oligomerization process *in vitro* directly related to the presence of the HRR. The X-ray structure of a truncated version lacking the C-terminus revealed the existence of an additional metal-binding site at the dimer interface, which binds Ni(II) with an affinity of 380 nM through a $H_{18}XXXH_{22}XXXH_{26}$ motif [8]. In the 46 identified homologs, the HF/WXXHXXXH motif is strictly conserved, while the presence and the length of the C-terminal His tail is variable. *Rr*CooJ possesses thus independent and spatially separated Ni-binding sites: C-terminal histidine tails that bind Ni(II) with a K_D of 1.6 µM, and a high affinity site (HAS) located in the coiled coil.

In the present study, we broadened the investigation of the CooJ family through a search for *Rr*CooJ homologs. The results support the existence of more than 150 members belonging to this family in bacteria and archaea, co-occuring or not with CODH and/or CooC and/or CooT. The presence of the His tail was observed either at the N- or at the C-terminus, with variable length and composition. In addition, this study revealed that the HAS motif is not strictly conserved, varying in terms of histidine content (2, 3 or 4) and sequence. To validate the memberships of the CooJ family, three representative CooJ-like proteins were produced, purified, and characterized: i) CooJ from *Treponema azotonutricium* (*Ta*CooJ) with an N-terminal HRR and a **Y**XXX**H**NXX**H** motif, ii) CooJ from *Methanococcoides burtonii* (*Mb*CooJ) with no HRR and a **H**XXX**H**WXX**H**XXX**H** motif, and iii) CooJ from *Shewanella*

*fodinae (Sf*CooJ) with a short N-terminal HRR and a **H**W**H**X**H**NXX**H** motif. Homology models were built from the truncated *Rr*CooJ structure, while the behavior of the three proteins towards Ni(II) was evaluated by biophysical approaches and compared to that of *Rr*CooJ.

2. Material and methods

2.1 Search for CooJ homologues

Homologues of CooJ from *R. rubrum* S1 (Q2RUG4_RHORT) sequence were identified with the blastP program (https://blast.ncbi.nlm.nih.gov/Blast.cgi) [13], [14], using a non-redundant protein database (v 2019_11) limited to bacterial taxa, and applying default parameters (threshold 0.05, Blosum62 Matrix). This approach allowed the identification of six CooJ homologues (WP_011389184.1 hypothetical protein [*Rhodospirillum rubrum*], WP_184262707.1 hypothetical protein [*Rhodopseudomonas rhenobacensis*], WP_011474896.1 hypothetical protein [*Rhodopseudomonas palustris*], WP_158913189.1 hypothetical protein [*Caulobacter sp*. S45], SCM76168.1 putative CooJ [uncultured *Pleomorphomonas sp*.] and WP_100079579.1 hypothetical protein [*Pleomorphomonas carboxyditropha*]). CooJ homologues were then aligned with the MAFFT program (version v6.864; L-INS-i option; default parameters) [15], [16] (https://www.genome.jp/tools-bin/mafft). This set of sequences was used to quarry the database Reference proteomes (v.2019_09) with the HMMSEARCH program (Hmmer Web version 2.41.1 https://www.ebi.ac.uk/Tools/hmmer/search/hmmsearch) [17], [18]. Hits with e-values < 0.3 and sequences with e-values < 0.1 were retrieved and aligned with MAFFT. The procedure was repeated twice, until no additional CooJ homologue could be detected. A multiple sequence alignment was performed with ClustalW and used to generate a Hidden Markov Model (HMM) profile with the HMMBUILD program (https://npsa-prabi.ibcp.fr/cgi-bin/npsa_automat.pl?page=/NPSA/npsa_hmmbuild.html) [19], [20]. The web application Skyline [21] was then used to generate the HMM logos. A representation with amino acid residues above background has been selected. To generate sequence similarity plots, multiple sequence alignments were obtained with MAFFT [15], [16] as stated above, and a distance matrix was calculated using protdist in the PHYLIP package [22] with the Kimura distance as a criterion for similarity. A cutoff of 1.3 was used to define an interaction in the sequence similarity plot and for the few cases where the distances were too high to be handled by the Kimura model, the -1 values were simply replaced by 0. The yED Graph Editor (Version 3.20 Powered by the yFiles Graph Visualization Library http://www.yWorks.com) was used for

clustering and displaying the similarity network with an organic layout. The Seaview program [23] was used as a graphical interface to align and plot the selected sequences (clustalo option).

2.2 Genomic context analysis

Genomic context analysis was performed using the tools and annotation of KEGG Genes Database (https://www.kegg.jp/kegg/genes.html), GenBank at NCBI (https://www.ncbi.nlm.nih.gov/), PATRIC 3.6.7 (https://www.patricbrc.org/) as well as Uniprot (https://www.uniprot.org/). Most genes are re-annotated manually in order to correct for erroneous annotations or to homogenize the annotations. For example *cooS* is used for monofunctional CODH and *acsA* for bifunctional CODH/ACS. The genes for CooC-type proteins are annotated *cooC* or *acsF* if they are homologous to *Carboxydothermus hydrogenoformans cooC1/C3* or *cooC2*, respectively (Gregg, C. M. et al 2016, J. Biol. Chem. 291, 18129–38). The genes encoding proteins annotated CbiM, N, O or Q were re-annotated *nik* as the proteins are more homologous to Nik proteins from *Rhodobacter capsulatus* than to Cbi protein [24]. The genes annotated *fdhA* can in fact correspond to two different domains of the FdhA protein.

2.3 Homology model building

The search for remote homologous sequences with known structure to be used as template to build homology models of *Ta*CooJ, *Mb*CooJ and *Sf*CooJ was carried out using the MPI Bioinformatics Toolkit web server (https://toolkit.tuebingen.mpg.de) [25]. Each sequence was used as input for a template search using the HHpred method [26], [27], [28]. A multiple sequence alignment (MSA) of the query sequence was built using three iterations of HHblits [28] over UniRef30 [29], a version of the UniRef sequence database [30] clustered into groups of similar sequences at a length coverage of at least 80% and a maximum pairwise sequence identity of 30%. The obtained MSA was annotated with the predicted secondary structure using PSIPRED [31] and converted to a HMM profile using three iterations of HHblits over the UniRef30 database. The obtained query MSA was compared to each HMM profile in the PDB_mmCIF70 structural database (a subset of the Protein Data Bank filtered for a maximum pairwise sequence identity of 70%) built using the same method as for the query MSA. The database matches were ranked based on the probability of the match to be homologous to the target sequence using the default parameters, to distinguish homologous from non-homologous matches. HHpred thus provided a list of the closest homologs, with pairwise alignments. The template with the highest estimated probability (99.9%) was *Rr*CooJ (PDB code 6HK5) in all

three cases, with sequences covering residues 18-85, 1-69 and 12-78 for *Ta*CooJ, *Mb*CooJ and *Sf*CooJ respectively. This template was selected in all three cases, and each alignment was forwarded, using the MPI Bioinformatics Toolkit server, to MODELLER [32] for structure homology modelling. Each of the three models thus produced was used as input for YASARA [33] in order to extend the missing N-terminal and C-terminal protein portions by considering the anchor atoms for the terminal five residues, optimizing the backbone and side chains conformation through a search of the PDB for 200 samples, and minimizing the energy according to the YASARA2 force field.

2.4 Size exclusion chromatography coupled to multi-angle laser light scattering (SEC-MALLS)

Purified and frozen CooJ proteins were thawed prior to injection onto the SEC-MALLS system (Wyatt Dawn HELEOS-II 18-angle light scattering detector and Wyatt Optilab rEX refractive index monitor linked to a Shimadzu HPLC system comprising a LC-20AD pump, a SPD20A UV/Vis detector, and a Superdex 200 10/300 increase column (GE Healthcare Life Sciences, Pittsburg, USA). Injections were carried out using a 20 µL loop. Ni-CooJ proteins were prepared by incubation of apo-CooJ at 50 µM dimer with 0, 50, 100 or 150 µM $NiSO_4$ for 30 min at room temperature and centrifuged at 15 000 rpm for 5 minutes prior to injection onto the SEC-MALLS system (Wyatt Dawn HELEOS-II 18-angle light scattering detector and Wyatt Optilab rEX refractive index monitor linked to a Shimadzu HPLC system comprising a LC-20AD pump, a SPD20A UV/Vis detector, and a Superdex 200 10/300 increase column (GE Healthcare Life Sciences, Pittsburg, USA). Injections were carried out using a 20 µL loop. The size exclusion column was equilibrated using 50 mM 4-(2-hydroxyethyl)-1-piperazineethanesulfonic acid (HEPES) pH 7.5, 300 mM NaCl, 1 mM tris(2-carboxyethyl)phosphine (TCEP) (buffer A2) for apo-CooJ proteins and buffer A2 ± 10 µM $NiSO_4$ for Ni-CooJ proteins. The size exclusion column was equilibrated using buffer A2. Protein concentration in all samples was precisely determined by integration of the differential refractive index (dRI) peak (dn/dc = 0.185). The data were analyzed using the ASTRA software (version 6) (WYATT Technology Corporation, Santa Barbara, USA).

2.5 Circular dichroism (CD) spectroscopy

CD spectra were recorded using a J-1500 circular dichroism spectrometer from JASCO Analytical Instruments. A stock solution of 10 mM $NiSO_4$ was used to monitor metal-ligand charge transfer and d-d transitions of the three CooJ proteins (0 and 3 molar equivalents of

$NiSO_4$). Spectra were recorded from 250 to 700 nm using a 10 mm cuvette, with ten accumulations to increase the signal-to-noise ratio. Proteins were thawed and diluted to 25-100 µM dimer in buffer A2. CD spectra were also recorded using a 1 mm cuvette in the 190-250 nm range to determine the secondary structure content in the absence or in the presence of 4 molar equivalents of $NiSO_4$, with ten accumulations on samples containing 10 µM protein dimer in CD buffer (6 mM HEPES pH 7.5, 10 mM NaCl). The spectra were analyzed using the JASCO spectra manager software (version 2).

2.6 Isothermal titration calorimetry (ITC)

Ni(II) binding titrations of CooJ proteins were performed at 25 °C using a high-sensitivity VP-ITC microcalorimeter (MicroCal, Northampton, MA, USA). The protein and the metal ion salt ($NiSO_4$) were diluted to 15 µM (monomer) and 250 mM respectively into a solution of buffer A2. The reference cell was filled with deionized water. Before each experiment, the baseline stability was verified. An interval of five minutes was applied between the injections to allow the system to reach thermal equilibrium. Control experiments were conducted by titration of the metal ion solution into the buffer alone under identical conditions, and the heat of dilution was negligible. The solution containing the protein was loaded into a sample cell (1.4093 mL) and was titrated with 30 x 10 µL injections with the nickel solution. The integrated data were fit with the Origin software package (MicroCal), using a nonlinear least-squares minimization algorithm to theoretical titration curves with different binding schemes.

The values for the enthalpy change of the reaction (ΔH), the binding affinity constant (K_D), and the number of sites (n) were parameters of the fit. The reaction entropy was calculated using $\Delta G = - RT\ln K$ ($R = 1.9872$ cal mol^{-1} K^{-1}, $T = 298$ K) and $\Delta G = \Delta H - T\Delta S$. The values given for ΔH and ΔS are apparent values, and include contributions not only from metal binding but also from associated events such as protonation/deprotonation of the amino acid residues involved in binding and the consequent change in the buffer ionization state.

3 Results and discussion

3.1 CooJ homologues possess diverse putative metal-binding motifs

The search for CooJ homologues led to a set of 152 proteins within Reference Proteomes (Table S1). As detailed in Table 1, these proteins were predominantly found in the bacterial kingdom, but also in Archaea. In the latter case, CooJ homologues were only identified in the Euryarchaeota phylum, while in bacteria several phyla are concerned with a high representation

of Firmicutes and Proteobacteria. While the HAS motif was previously proposed to be strictly conserved, sequence alignments revealed variations in its sequence and histidine content. Based on this analysis, three distinct motifs were identified: the "3H" motif (HXXXHXXXH), found in bacteria, the "4H" motif (HXXXHWXXHXXXH), found in Archaea, and the "Y2H" motif (YXXXHXXXH), mainly found in bacteria (Table 1, Fig. 1).

The "3H" motif group

This pattern corresponds to the one identified in *Rr*CooJ [8] and is considered as the standard motif. This group comprises 81 bacterial protein sequences mostly found in Firmicutes and Proteobacteria (Table 1). Concerning the HRR, 13 sequences possess a C-terminal His tail as observed in *Rr*CooJ. In 48 sequences, the His tail is present at the N-terminus and 20 proteins do not possess any HRR (Fig. S1 and Table 2). Note that one protein (A0A0U5AMG9_9BACT) should have been in the "4H" motif group (see below) but is more similar to proteins in the 3H group. An HMM logo was generated for the core domain and is shown in Fig. 1A. It is worth mentioning that a few specific patterns can be detected with extra histidine residues within this motif, (Fig. S2), as observed in *Sf*CooJ.

The "4H" motif group

In this group, the motif contains an extra histidine residue, located three residues upstream of the first histidine of the "3H" motif (Fig. 1B). The sequences all belong to Archaea with the exception of the A0A0U5AMG9_9BACT sequence, which belongs to the "3H" motif group. Indeed, the bacterial sequence does not possess the strictly conserved tryptophan residue following the second histidine (HXXXH**W**XXHXXXH). This motif is the most common found in Archaea. The 15 sequences were all identified in the Euryarchaeota phylum (Table 1), As shown in Fig. S3 and Table 2, a HRR is rarely observed, as illustrated by the sequence of *Mb*CooJ, with only two examples possessing a short N-terminal tail containing a small number of histidines (Table S2).

The "Y2H" motif group

Among the 152 proteins identified, 48 sequences possess a conserved motif with two histidine residues. In this case, a tyrosine is strictly conserved three residues upstream of the first histidine, as shown in the generated HMM logo (Fig. 1C). The motif is mainly encountered in Bacteria (only one Archaea) and mostly in Firmicutes (43) (Table 1). As shown in Fig. S4, this group can be subdivided with the YXXXHNXXH found in 15 sequences and the YXXXHNXHH possessing an extra-histidine in 33 sequences, the latter being present in 29 Firmicutes. It was also possible to detect a conserved motif at the N-terminus of 34 sequences

as shown in Fig. S4 and in the HMM logo (Fig. S5**)**. Thirty sequences possess both the conserved N-terminal and the "YX_3HNXHH" motifs. However, this N-terminal motif does not match any known pattern. All but one sequence (A0A2V3JGC3_9EURY) possess an N-terminal HRR (Table 2), as in *Ta*CooJ. In both "3H" and "Y2H" groups, N-terminal extensions often contain several cysteine residues and frequently in combination with glycine residues (Fig. S6). This pattern is even more frequent in the "Y2H" motif group.

The similarity plot for the three types of CooJ motifs (Fig. S7) clearly shows that the "Y2H" group is relatively well separated from the "3H" and "4H" groups. Note also that when several CooJ proteins are present in a species (for example, *Clostridium magnum* possesses three CooJ), they all belong to the same group.

Unclassified CooJ homologues

Five proteins possess only the two last histidine residues of the "3H" motif, positioned at the N-terminus of the sequences. However, by translating the bases upstream of the initial methionine, a potential HW motif could be identified in A0A0F2J063_9BACT and a Y residue in F5YMP3_TREPZ, A0A0J1GDY4_9FIRM, C6LCL5_9FIRM and R6G788_9FIRM, which could give rise to the "3H" and "Y2H" motifs. This suggests rather an error in the identification of the start codon, but nonetheless these sequences were not included in the Logo generation or other analyses. On the other hand, three proteins possess a long N-terminal extension, not particularly rich in histidines. Two of them are archaeal proteins (A0A1F2P6W7_9EURY and A0A1F2PB93_9EURY) with a "4H" or a "3H" motif, respectively and are fused with a Mut7C RNAse domain, often related to an endonuclease function or implicated in tRNA maturation. The third one (A0A2U3QHE2_9BACT), found in *Candidatus Sulfobium mesophilum*, is a fusion between a NikO homologue and CooJ. Interestingly, this protein is found downstream NikMN and NikQ homologues, all involved in nickel import.

3.2 Genomic context of CooJ homologues

In most of the cases, CooJ homologues are found in gene clusters with bifunctional CODH/ACS or monofunctional CODH (Fig. 2, S9-10). CooJ are encountered in clusters of various size with the bifunctional ACS/CODH in 45% of the cases and only 4% in clusters encoding the monofunctional CooS. In some cases, the CooJ/CODH/ACS cluster also contains genes for proteins involved in acetogenesis such as the formate-tetrahydrofolate ligase or the methylene-tetrahydrofolate reductase. However, CooJ can also be identified either isolated from other Coo proteins, or in duo with CooT or in trio with CooT and CooC (Fig. 2, S8-10, Table S2). Sometimes, CooJ is also found next to the heterodisulfide reductase involved in methanogenesis

in methanogens or to the *nikMNQO* operon, involved in nickel import in bacteria. Isolated CooJ represent about 30% of the genomes including archaeal CooJ that are always isolated from the genes encoding CODH or maturation proteins. In addition, genes encoding for proteins with a DUF3842 domain as determined in Pfam are encountered next to "3H" motif- containing CooJ (Fig. 2) in more than 30% of the cases but never with the "4H" or Y2H motifs and mostly in Firmicutes.

3.3 Comparative modeling of TaCooJ, MbCooj and SfCooJ

In order to validate the memberships of the CooJ family, three representatives CooJ proteins were selected for structural homology modeling: *Sf*CooJ, possessing the standard "3H" motif including an extra histidine, *Mb*CooJ to illustrate the archaeal "4H" group, and *Ta*CooJ that belongs to the "Y2H" group. Secondary structure predictions (using PSIPRED and DISOPREP3) revealed that, like *Rr*CooJ, the three CooJ are mainly composed of α-helices and a disordered region, mostly corresponding to the His tail (Fig. 3A). In a second step, the homology models of *Ta*CooJ, *Mb*CooJ and *Sf*CooJ (Fig. 3B) were produced and superimposed to the X-ray structure of *Rr*CooJ, which is missing the His tail (PDB code: 6HK5). The missing N-terminal residues MGSHHTHHHDH of *Sf*CooJ were added to the model: the His25/His27/His29/His33 motif resembles the His18/His22/His26 motif of *Rr*CooJ with the additional His27 corresponding to Leu20 in *Rr*CooJ. There are six additional His at the N-terminus as potential Ni-binding residues. From the amino acid sequence, *Mb*CooJ is predicted to possess one putative nickel-binding motif involving His12, His16, His20 and His24. The superposition of the *Mb*CooJ model with the *Rr*CooJ structure shows their correspondence with Ile14, His18, His22 and His26 in *Rr*CooJ, respectively. In *Ta*CooJ, the missing N-terminal residues MGHDDHGKPHDHHDHEH were added. Overlap of this model with *Rr*CooJ shows that the "Y2H" motif (Tyr32/His36/His40) matches well with the "3H" motif of *Rr*CooJ (His18/His22/His26). In *Ta*CooJ there are three additional residues (His49, His52, His53) and seven additional His at the N-terminus as potential Ni-binding residues. This study suggests that the three distinct motifs identified in this study constitute the same metal-binding site, present in all homologues in the CooJ family. This characteristic could then be considered as a signature of this protein family. To further examine the capacity of the three proteins to bind Ni(II), as previously demonstrated for *Rr*CooJ, their biophysical characterization was undertaken.

3.4 Biophysical characterization of SfCooJ, MbCooJ and TaCooJ.

The three CooJ proteins were successfully overproduced in *E. coli* and purified (protocols are detailed in SI). Disulfide bond formation was prevented by addition of 1 mM TCEP in all buffers. Their molecular masses were determined using ESI-MS, which revealed that the three proteins were purified mostly as Met1-lacking forms containing an additional glycine at the N-terminus coming from the cloning procedure **(**Fig. S11). Like *Rr*CooJ, *Sf*CooJ, *Mb*CooJ and *Ta*CooJ are dimeric in solution, as shown by SEC-MALLS with main eluted peaks of ~21 kDa, ~17 kDa and ~20 kDa, respectively (Fig. S12). Circular dichroism (CD) spectroscopy in the far-UV range shows the typical signature of α-helical proteins, with a positive peak at ~ 195 nm and two negative peaks at ~ 205 and ~ 220 nm (Fig. 4A), as previously observed for *Rr*CooJ and in agreement with the homology models.

With the aim to investigate the ability of the three CooJ to bind Ni(II), CD spectroscopy measurements in the near-UV and visible ranges were carried out. Upon addition of Ni(II) to the three apo-CooJ, a ligand-to-metal charge transfer appeared at ~270 nm (-), likely due to the binding of Ni(II) to histidine residues. In the case of *Sf*CooJ, additional absorption bands were observed in the 450-500 nm region (-) and at ~420 nm (+) (Fig. 4B). These results strongly suggest that the three CooJ proteins are able to bind Ni(II).

In order to study the impact of Ni(II) on *Ta*CooJ, *Mb*CooJ and *Sf*CooJ oligomerization, SEC-MALLS experiments were conducted using each CooJ pre-incubated with 0, 1, 2 and 3 eq. of $NiSO_4$ per dimer for 30 minutes at room temperature prior to injection. Unlike *Rr*CooJ [34], the three proteins do no tend to form higher oligomers upon Ni addition: *Ta*CooJ forms always a dimer, regardless of the Ni concentration. The presence of Ni(II) slightly increased the elution volume of Ni(II)-*Ta*CooJ compared to the apo-protein, suggesting that metal binding induces a modification of the hydrodynamic properties of *Ta*CooJ. *Sf*CooJ and *Mb*CooJ tend to form tetramers upon addition of 1 equivalent of Ni(II), with elution peaks likely corresponding to a mixture of dimers and tetramers, (Fig. 4C). The addition of a Ni(II) excess led to protein precipitation, as shown by the decreasing protein concentration according to Ni(II) concentration (from 51 µM to 35 µM for *Ta*CooJ, from 49 µM to 26 µM for *Mb*CooJ and from 45 µM to 20 µM for *Sf*CooJ).

Titration of *Ta*CooJ, *Mb*CooJ and *Sf*CooJ using isothermal titration calorimetry (ITC) showed negative peaks following Ni(II) additions for all three proteins, indicative of exothermic events (Fig. 5A, B, C). For *Ta*CooJ, the shape of the binding isotherm (Fig. 5D) resulting from the integration of the heat peaks showed two different slopes, indicative of two binding events in different sites, prompting the application of a binding model that involves two sets of sites for calorimetric data fitting and interpretation. The first binding event occurs with a half integer

stoichiometry, indicative of the binding of a metal ion per dimer, with an affinity in the sub-micromolar range (K_{D1} = 0.16 μM), and is enthalpy and entropy driven (Table 3). The second binding event shows a lower affinity in the micromolar range (K_{D2} = 3.2 μM), a favorable enthalpic factor and an unfavorable entropy (Table 3). Differently, the binding curve of *Mb*CooJ presents a unique slope, indicative of a single binding event (Fig. 5E). A fit of the thermodynamic data indicated the interaction of one Ni(II) per monomer with the affinity in the micromolar range (K_D = 0.5 μM), mainly enthalpy driven and with a minor positive entropic factor (Table 3). Finally, *Sf*CooJ presents a bipartite binding isotherm that was fitted with a model involving two sets of independent sites (Fig. 5F). The first binding event of one Ni(II) per dimer occurs with an affinity above the ITC detection limit (K_{D1} < 0.1 nM); therefore, it was necessary to fix the value of the affinity constant during the fitting procedure in order to allow the fit to go to convergence. This high affinity binding showed favorable enthalpic and entropic factors (Table 3). The second binding event of one Ni(II) per monomer occurs with affinity in the micromolar range (K_{D2} = 8 μM) and is enthalpy driven with a negative entropic factor (Table 3). The ITC data obtained for *Ta*CooJ and *Sf*CooJ recall the situation previously reported for *Rr*CooJ[8], showing two metal binding sites, with one Ni(II) ion bound with higher affinity in sub-micromolar range and half-integer stoichiometry and a second Ni(II) binding event occurring with lower affinity in the micromolar range. As observed for *Rr*CooJ, for which Ni(II) titration was performed both on the native protein and on a protein variant lacking the C-terminal HRR, for both *Ta*CooJ and *Sf*CooJ the high affinity binding event most likely occurs at the dimer interface, likely involving the Y2H or the 3H metal binding sites, respectively. Interestingly, the binding signatures are conserved when compared to *Rr*CooJ: the first metal binding event occurs with favorable enthalpic and entropic factors, while Ni(II) binding to the HRR is enthalpically-driven and shows a negative entropy of binding. This latter observation might reflect the induction of some rigidity in the disordered tail upon metal binding. Notably, *Mb*CooJ, which does not show any N- or C-terminal HRR, presents a unique metal binding site with the characteristics of the high affinity binding sites.

4. Conclusions

Until a few years ago, the accessory protein CooJ, involved in the biosynthesis of the active site of CODH, were only found in in two bacterial species, i.e. *R. rubrum* and *Rhodopseudomonas palustris*. Consequently, this nickel chaperone has long been regarded as playing a minor role in the maturation pathway of the enzyme. In the last two decades, genome sequencing has

dramatically increased in speed and efficiency, allowing the identification of whole genome sequences of a multitude of microorganisms. In this study, access to update proteome databases has led to the discovery of more than 150 non-redundant CooJ sequences in bacteria and archaea. Regarding their genomic contexts, *cooJ* genes are often found close to gene clusters encoding bifunctional or monfunctional CODH. However, they can also be found isolated in the genome, as observed in methanogens, or in duo or trio with the two other accessory proteins involved in CODH maturation, namely CooT and CooC. Based on their amino-acid sequences, CooJ proteins can be regrouped in the same family. The X-ray structure and characterization of *Rr*CooJ revealed two independent Ni(II)-binding sites: a high-affinity site and a C-terminal histidine tail. Here, we showed that the HAS is not strictly conserved with three different possible motifs and that the Histidine tail is mostly present at the N-terminus or absent. Three representative CooJ were purified and characterized, namely *Ta*CooJ, *Mb*CooJ and *Sf*CooJ. Their homology models suggest a coiled coil topology, comparable to the structure of *Rr*CooJ. Like *Rr*CooJ, they form dimers in solution and possess at least one Ni(II)-binding site with an affinity in the sub-micromolar range. Differently, they do not form Ni(II)-dependent high-order oligomers, as observed with *Rr*CooJ. Altogether, these studies have provided substantial information about the potential role of CooJ in nickel trafficking. Further studies are required to clarify the precise role of CooJ in CODH maturation or in other metabolic processes.

Acknowledgements

This work was supported by the Agence Nationale de la Recherche through the LabEx ARCANE program (ANR-11-LABX-0003-01) and the Graduate School on Chemistry, Biology and Health of Univ Grenoble Alpes CBH-EUR-GS (ANR-17-EURE-0003)
We thank Dr. Luca Signor (Institute for Structural Biology, Grenoble, France) for MS experiments in denaturing conditions (Integrated Structural Biology Grenoble platform).
This work used the SEC-MALLS Platform with support from GRAL (ANR-10-LABX-49-01).
The research at the Laboratory of Bioinorganic Chemistry of the University of Bologna (BZ and BSCZ) is supported by the Consorzio Interuniversitario di Risonanze Magnetiche di Metallo-Proteine (CIRMMP).

Legends to figures

Figure 1: HMM logos for the three groups of CooJ HAS as determined in this study. (A) "3H" motif; (B) "4H" motif and (C) "Y2H" motif.

Figure 2: Genomic contexts of representative CooJ homologues (see Figure S8 for protein nomenclature). Most of the genes were manually annotated in order to correct misannotated genes or to homogenize the annotations.

Figure 3: (A) Aminoacid sequences of recombinant *Rr*CooJ, *Sf*CooJ, *Mb*CooJ and *Ta*CooJ. The predicted helix and the disordered region are shown in blue and dashed boxes, respectively. The predicted high affinity motifs are boxed in dark blue. Histidines are in red. (B) Homology models of *Sf*CooJ, *Mb*CooJ and *Ta*CooJ based on the crystal structure of truncated *Rr*CooJ (PDB code: 6HK5). The figures were made with PyMOL (The PyMOL molecular graphic system, Version 2.5.0 Schrödinger, LCC)

Figure 4: (A) CD measured in the far-UV region (190-250 nm). Spectra in the 190–250-nm range shows the secondary structure composition of the protein in solution. The apo-protein spectra were recorded at 10 µM dimer concentration in 6mM HEPES, pH 7.5, 10mM NaCl. (B) CD measured in the near-UV visible region (250-600 nm). SfCooJ and MbCooJ were at 25µM M dimer and TaCooJ at 50 µM dimer pre-incubated 15 minutes with 0 or 3 molar eq. of $NiSO_4$. The buffer contained 50 mM HEPES, pH 7.5, 300 mM NaCl, 1 mM TCEP (C) Characterization of the Ni(II)-induced oligomerisation of *Sf*CooJ, *Mb*CooJ and *Ta*CooJ. Chromatograms of SEC-MALLS analysis of the three CooJ proteins in the presence of of Ni(II) (from 0 to 3 molar eq). Apo-protein samples were injected at 50 µM dimer, and a stock solution of 1mM $NiSO_4$ was added to reach 0 to 3 molar eq. (0 to 150 µM). The chromatograms are in red (0 Ni eq.), cyan (1 Ni eq.), blue (2 Ni eq.) and magenta (3 Ni. Eq.)

Figure 5. Representative raw plots of the ITC data of Ni(II) (250 mM) injected onto the (A) *Ta*CooJ (B) *Mb*CooJ and (C) *Sf*CooJ solutions (15 µM). Integrated heat data as a function of the metal-to-protein molar ratio for (D) *Ta*CooJ (E) *Mb*CooJ and (F) *Sf*CooJ. The continuous lines represent the best fit obtained using a model involving a single set (*Mb*CooJ) or two independent sets of binding sites for Ni(II) (*Ta*CooJ and *Sf*CooJ), as described in the text.

References

[1] M. Alfano, C. Cavazza, Structure, function, and biosynthesis of nickel-dependent enzymes, Protein Sci. (2020) pro.3836. doi:10.1002/pro.3836.
[2] L. Domnik, M. Merrouch, S. Goetzl, J.H. Jeoung, C. Léger, S. Dementin, V. Fourmond, H. Dobbek, CODH-IV: A High-Efficiency CO-Scavenging CO Dehydrogenase with Resistance to O2, Angew. Chemie - Int. Ed. 56 (2017) 15466–15469. doi:10.1002/anie.201709261.
[3] C.L. Drennan, J. Heo, M.D. Sintchak, E. Schreiter, P.W. Ludden, Life on carbon monoxide: X-ray structure of Rhodospirillum rubrum Ni-Fe-S carbon monoxide dehydrogenase, Proc. Natl. Acad. Sci. U. S. A. 98 (2001) 11973–11978. doi:10.1073/pnas.211429998.
[4] B. Roche, L. Aussel, B. Ezraty, P. Mandin, B. Py, F. Barras, Iron/sulfur proteins biogenesis in prokaryotes: Formation, regulation and diversity, Biochim. Biophys. Acta - Bioenerg. 1827 (2013) 455–469. doi:10.1016/j.bbabio.2012.12.010.
[5] W.B. Jeon, S.W. Singer, P.W. Ludden, L.M. Rubio, New insights into the mechanism of nickel insertion into carbon monoxide dehydrogenase: Analysis of Rhodospirillum rubrum carbon monoxide dehydrogenase variants with substituted ligands to the [Fe3S4] portion of the active-site C-cluster, J. Biol. Inorg. Chem. 10 (2005) 903–912. doi:10.1007/s00775-005-0043-z.
[6] J.H. Jeoung, T. Giese, M. Grünwald, H. Dobbek, Crystal structure of the ATP-dependent maturation factor of Ni,Fe-containing carbon monoxide dehydrogenases, J. Mol. Biol. 396 (2010) 1165–1179. doi:10.1016/j.jmb.2009.12.062.
[7] J.H. Jeoung, T. Giese, M. Grünwald, H. Dobbek, CooC1 from Carboxydothermus hydrogenoformans is a nickel-binding ATPase, Biochemistry. 48 (2009) 11505–11513. doi:10.1021/bi901443z.
[8] M. Alfano, J. Pérard, P. Carpentier, C. Basset, B. Zambelli, J. Timm, S. Crouzy, S. Ciurli, C. Cavazza, The carbon monoxide dehydrogenase accessory protein CooJ is a histidine-rich multidomain dimer containing an unexpected Ni(II)-binding site, J. Biol. Chem. 294 (2019) 7601–7614. doi:10.1074/jbc.RA119.008011.
[9] R.K. Watt, P.W. Ludden, The Identification, Purification, and Characterization of CooJ, J. Biol. Chem. 273 (1998) 10019–10025. doi:10.1074/jbc.273.16.10019.
[10] M. Alfano, J. Pérard, C. Cavazza, Nickel-induced oligomerization of the histidine-rich metallochaperone CooJ from Rhodospirillum rubrum, Inorganics. 7 (2019). doi:10.3390/INORGANICS7070084.
[11] J. Timm, C. Brochier-Armanet, J. Perard, B. Zambelli, S. Ollagnier-De-Choudens, S. Ciurli, C. Cavazza, The CO dehydrogenase accessory protein CooT is a novel nickel-binding protein, Metallomics. 9 (2017) 575–583. doi:10.1039/c7mt00063d.
[12] R.L. Kerby, P.W. Ludden, G.P. Roberts, In vivo nickel insertion into the carbon monoxide dehydrogenase of Rhodospirillum rubrum: Molecular and physiological characterization of cooCTJ, J. Bacteriol. 179 (1997) 2259–2266. doi:10.1128/jb.179.7.2259-2266.1997.
[13] S.F. Altschul, T.L. Madden, A.A. Schäffer, J. Zhang, Z. Zhang, W. Miller, D.J. Lipman, Gapped BLAST and PSI-BLAST: a new generation of protein database search programs, Oxford University Press, 1997.
[14] S.F. Altschul, J.C. Wootton, E.M. Gertz, R. Agarwala, A. Morgulis, A.A. Schäffer, Y.K. Yu, Protein database searches using compositionally adjusted substitution matrices, FEBS J. 272 (2005) 5101–5109. doi:10.1111/j.1742-4658.2005.04945.x.
[15] K. Katoh, K. Misawa, K.-I. Kuma, T. Miyata, MAFFT: a novel method for rapid multiple sequence alignment based on fast Fourier transform, n.d.
[16] K. Katoh, J. Rozewicki, K.D. Yamada, MAFFT online service: multiple sequence alignment, interactive sequence choice and visualization, 20 (2019) 1160–1166.

doi:10.1093/bib/bbx108.
[17] S.C. Potter, A. Luciani, S.R. Eddy, Y. Park, R. Lopez, R.D. Finn, HMMER web server: 2018 update, Web Serv. Issue Publ. Online. 46 (2018). doi:10.1093/nar/gky448.
[18] D506-D515, UniProt: a worldwide hub of protein knowledge The UniProt Consortium, Nucleic Acids Res. 47 (2019). doi:10.1093/nar/gky1049.
[19] S.R. Eddy, Profile hidden Markov models, n.d.
[20] P. Bucher, K. Karplus, N. Moeri, K. Hofmann, A flexible motif search technique based on generalized profiles, Comput. Chem. 20 (1996) 3–23. doi:10.1016/S0097-8485(96)80003-9.
[21] T.J. Wheeler, J. Clements, R.D. Finn, Skylign: a tool for creating informative, interactive logos representing sequence alignments and profile hidden Markov models, 2014.
[22] J. Felsenstein, PHYLIP - Phylogeny Inference Package (Version 3.2), Cladistics. (1989) 164–6.
[23] M. Gouy, S. Guindon, O. Gascuel, SeaView Version 4: A Multiplatform Graphical User Interface for Sequence Alignment and Phylogenetic Tree Building, Mol. Biol. Evol. 27 (2010) 221–224. doi:10.1093/molbev/msp259.
[24] F. Kirsch, T. Eitinger, Transport of nickel and cobalt ions into bacterial cells by S components of ECF transporters, (n.d.). doi:10.1007/s10534-014-9738-3.
[25] F. Gabler, S.Z. Nam, S. Till, M. Mirdita, M. Steinegger, J. Söding, A.N. Lupas, V. Alva, Protein Sequence Analysis Using the MPI Bioinformatics Toolkit, Curr. Protoc. Bioinforma. 72 (2020) 1–30. doi:10.1002/cpbi.108.
[26] J. Söding, Protein homology detection by HMM-HMM comparison, Bioinforma. Orig. Pap. 21 (2005) 951–960. doi:10.1093/bioinformatics/bti125.
[27] A. Hildebrand, M. Remmert, A. Biegert, J. Söding, Fast and accurate automatic structure prediction with HHpred, Proteins Struct. Funct. Bioinforma. 77 (2009) 128–132. doi:10.1002/prot.22499.
[28] M. Steinegger, M. Meier, M. Mirdita, H. Vöhringer, S.J. Haunsberger, J. Söding, HH-suite3 for fast remote homology detection and deep protein annotation, BMC Bioinformatics. 20 (2019) 1–15. doi:10.1186/s12859-019-3019-7.
[29] M. Mirdita, L. Von Den Driesch, C. Galiez, M.J. Martin, J.S.¨ Oding, M. Steinegger, Uniclust databases of clustered and deeply annotated protein sequences and alignments, Nucleic Acids Res. 45 (2017). doi:10.1093/nar/gkw1081.
[30] B.E. Suzek, Y. Wang, H. Huang, P.B. Mcgarvey, C.H. Wu, U. Consortium, UniRef clusters: a comprehensive and scalable alternative for improving sequence similarity searches, (n.d.). doi:10.1093/bioinformatics/btu739.
[31] D.T. Jones, Protein secondary structure prediction based on position-specific scoring matrices, J. Mol. Biol. 292 (1999) 195–202. doi:10.1006/jmbi.1999.3091.
[32] A. Sali, L. Potterton, F. Yuan, H. van Vlijmen, M. Karplus, Evaluation of Comparative Protein Modeling by MODELLER, 1995.
[33] E. Krieger, G. Vriend, J. Kelso, YASARA View-molecular graphics for all devices-from smartphones to workstations, Bioinforma. Appl. 30 (2014) 2981–2982. doi:10.1093/bioinformatics/btu426.
[34] M. Alfano, J. Pérard, C. Cavazza, Nickel-induced oligomerization of the histidine-rich metallochaperone CooJ from Rhodospirillum rubrum 3, 2019.

Table 1 Phylum distribution and classification of CooJ homologues

	Kingdom		Phylum	
152 CooJ homologues	18	Archaea	18	*Euryarchaeota*
	134	Bacteria	87	*Firmicutes*
			4	*Nitrospirae*
			2	*Planctomycetes*
			35	*Proteobacteria*
			2	*Spirochaetes*
			1	*Thermodesulfobacteria*
			1	*Thermodesulfobacteria*
			2	unclassified
81 "3H" motif	81	Bacteria	41	*Firmicutes*
			2	*Nitrospirae*
			2	*Planctomycetes*
			34	*Proteobacteria*
			1	*Thermodesulfobacteria*
			1	*Thermodesulfobacteria*
15 "4H" motif	15	Archaea	15	*Euryarchaeota*
48 "Y2H" motif	1	Archaea	1	*Euryarchaeota*
	47	Bacteria	43	*Firmicutes*
			1	*Proteobacteria*
			1	*Spirochaetes*
			2	unclassified
8 CooJ with ambiguous Nter and fused proteins	2	Archaea	2	*Euryarchaeota*
	6	Bacteria	3	*Firmicutes*
			2	*Nitrospirae*
			1	*Spirochaetes*

Table 2: Distribution of poly-His extensions according to the different motif groups.

Motif group		No His tail		N-terminal His tail		C-terminal His tail	
		Kingdom	Species	Kingdom	Species	Kingdom	Species
"3H" motif	**81**	**20** Bacteria	8 Firmicutes 2 Nitrospirae 1 Planctomycete 7 Proteobacteria 2 Thermodesulfobacteria	**48** Bacteria	33 Firmicutes 15 Proteobacteria	**13** Bacteria	1 Planctomycete 12 Proteobacteria
"4H" motif	**15**	**13** Archaea	13 Euryarchaeota	**2** Archaea	2 Euryarchaeota	**0**	
"Y2H" motif	**48**	**1** Archaea	1 Euryarchaeota	**47** Bacteria	43 Firmicutes 1 Proteobacterium 1 Spirochaete 2 unclassified	**0**	

Table 3: Thermodynamic parameters of Ni(II) binding to CooJ proteins

Experiments	N	K_A	K_D (μM)	ΔH (kcal mol^{-1})	ΔS (cal mol^{-1} K^{-1})	χ^2
***Ta*CooJ + Ni**	0.40 ± 0.02	6.0 ± 2x 10^6	0.16 ± 0.05	- 4.8 ± 0.2	14.8	5,602
	0.71± 0.05	3.1 ± 0.2 x 10^5	3.2 ± 0.2	- 13 ± 1	-20.0	
***Mb*CooJ + Ni**	1.16 ± 0.01	2.0 ± 0.1 x 10^5	0.50 ± 0.03	-8.26 ± 0.08	1.14	14430
***Sf*CooJ + Ni**	0.305 ± 0.008	1 x 10^{10}	0.0001	- 12.97 ± 0.01	2.24	3,000
	1.27 ± 0.1	8.3 ± 0.6 x 10^5	8 ± 3	- 10.53 ± 0.01	-8.23	

Scheme 1. C-cluster in CODH from *Rhodospirillum rubrum* (PDB code: 1JQK)

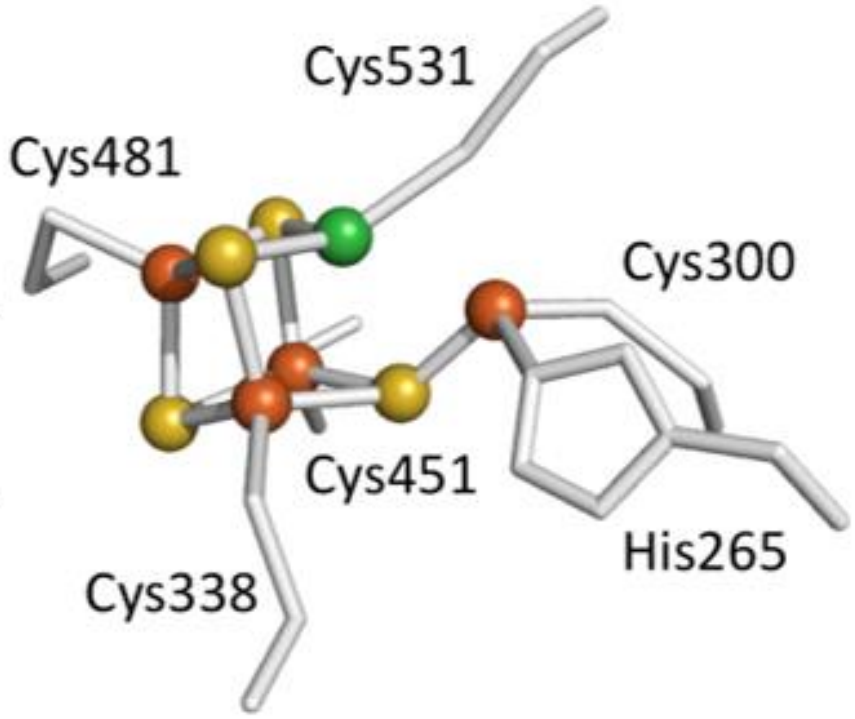

Figure 1

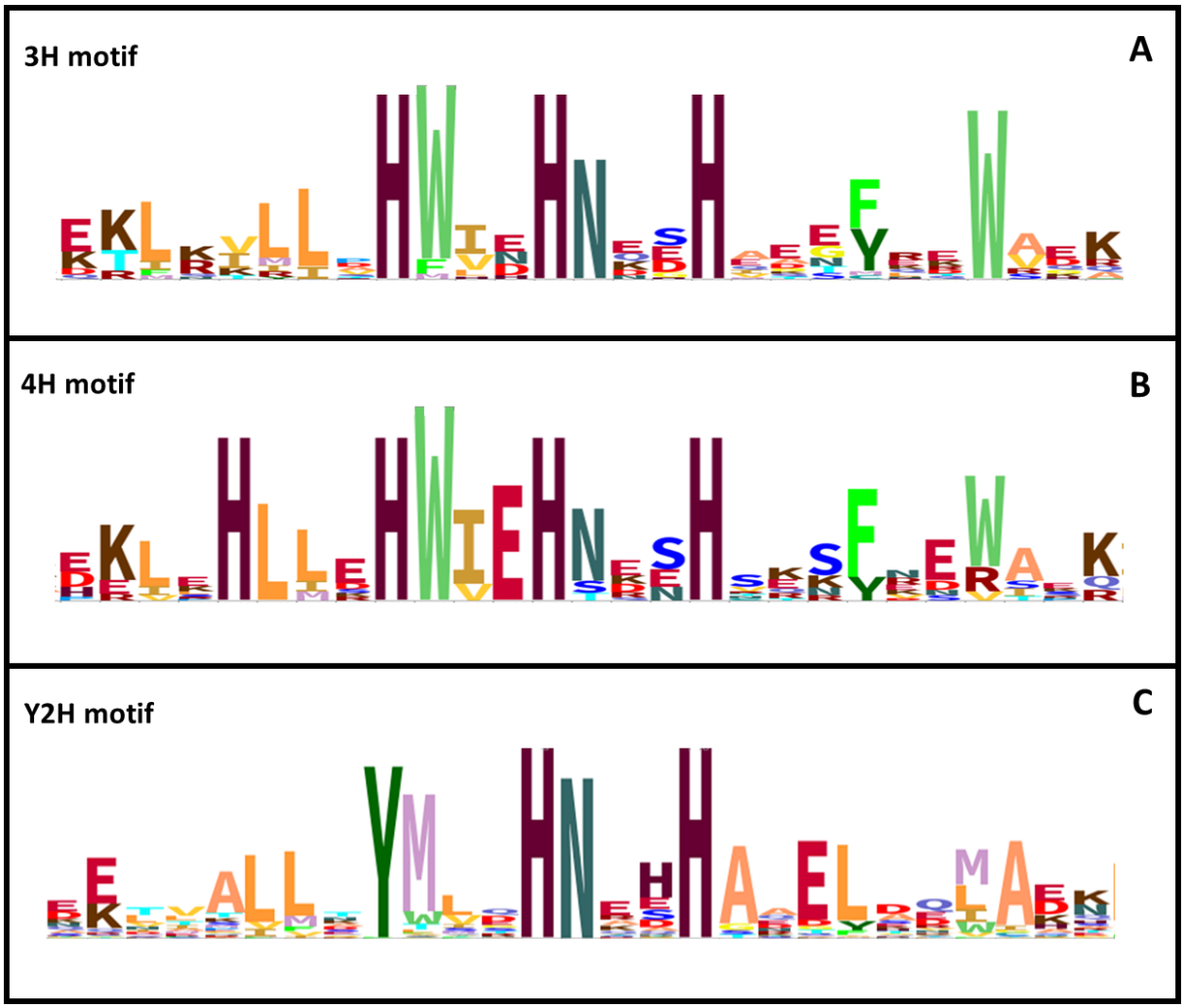

Figure 2:

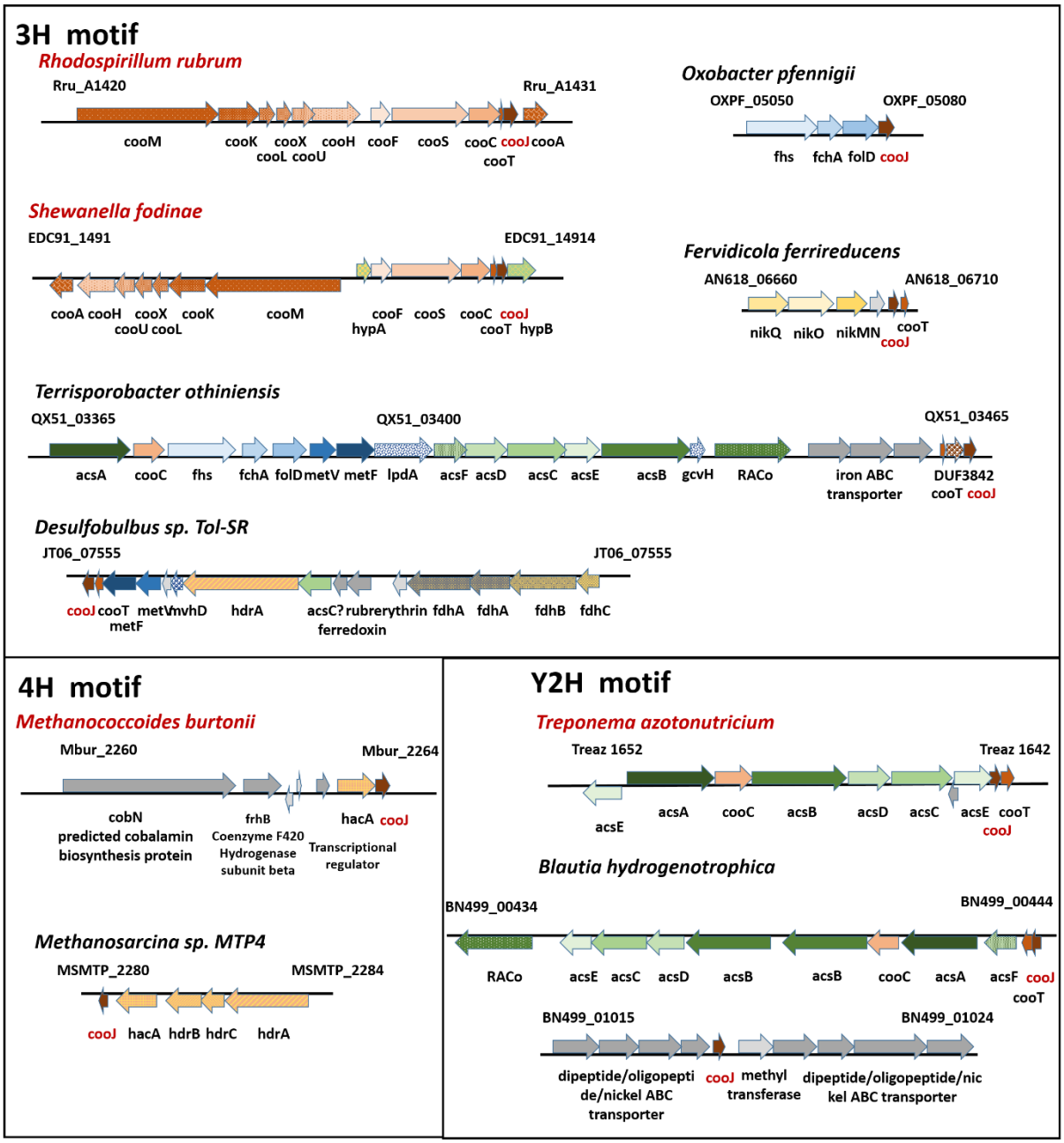
3H motif
Rhodospirillum rubrum
Rru_A1420
Rru_A1431
cooM
cooK cooX cooH cooF cooS cooC cooJ cooA
cooL cooU
cooT
Oxobacter pfennigii
OXPF_05050
OXPF_05080
fhs fchA folD cooJ
Shewanella fodinae
EDC91_1491
EDC91_14914
cooA cooH cooX cooK
cooU cooL
cooM
cooF cooS cooC cooJ
hypA
cooT hypB
Fervidicola ferrireducens
AN618_06660
AN618_06710
nikQ nikO nikMN
cooT
cooJ
Terrisporobacter othiniensis
QX51_03365
QX51_03400
QX51_03465
acsA cooC fhs fchA folD metV metF lpdA acsF acsD acsC acsE acsB gcvH RACo
iron ABC transporter
DUF3842 cooT cooJ
Desulfobulbus sp. Tol-SR
JT06_07555
JT06_07555
cooJ cooT metV metF
vhD
hdrA
acsC? rubrerythrin fdhA fdhA fdhB fdhC
ferredoxin
4H motif
Methanococcoides burtonii
Mbur_2260
Mbur_2264
cobN
predicted cobalamin biosynthesis protein
frhB
Coenzyme F420 Hydrogenase subunit beta
hacA cooJ
Transcriptional regulator
Methanosarcina sp. MTP4
MSMTP_2280
MSMTP_2284
cooJ hacA hdrB hdrC hdrA
Y2H motif
Treponema azotonutricium
Treaz 1652
Treaz 1642
acsE
acsA cooC acsB acsD acsC acsE cooT
cooJ
Blautia hydrogenotrophica
BN499_00434
BN499_00444
RACo acsE acsC acsD acsB acsB cooC acsA acsF cooJ
cooT
BN499_01015
BN499_01024
dipeptide/oligopeptide/nickel ABC transporter
cooJ methyl transferase
dipeptide/oligopeptide/nickel ABC transporter

Figure 3

A

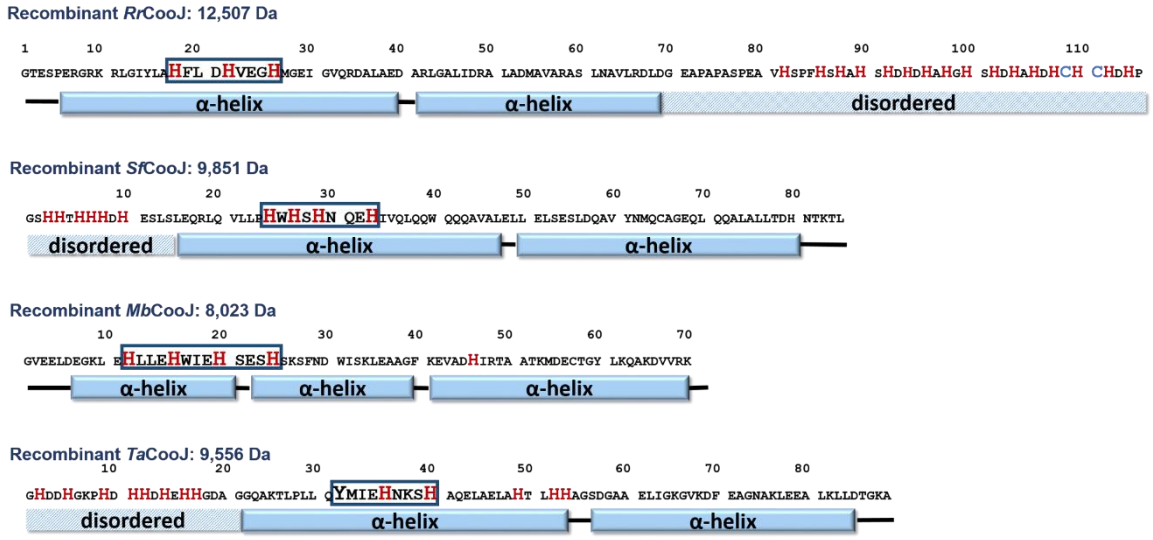
Recombinant RrCooJ: 12,507 Da
α-helix
α-helix
disordered
Recombinant SfCooJ: 9,851 Da
disordered
α-helix
α-helix
Recombinant MbCooJ: 8,023 Da
α-helix
α-helix
α-helix
Recombinant TaCooJ: 9,556 Da
disordered
α-helix
α-helix

B

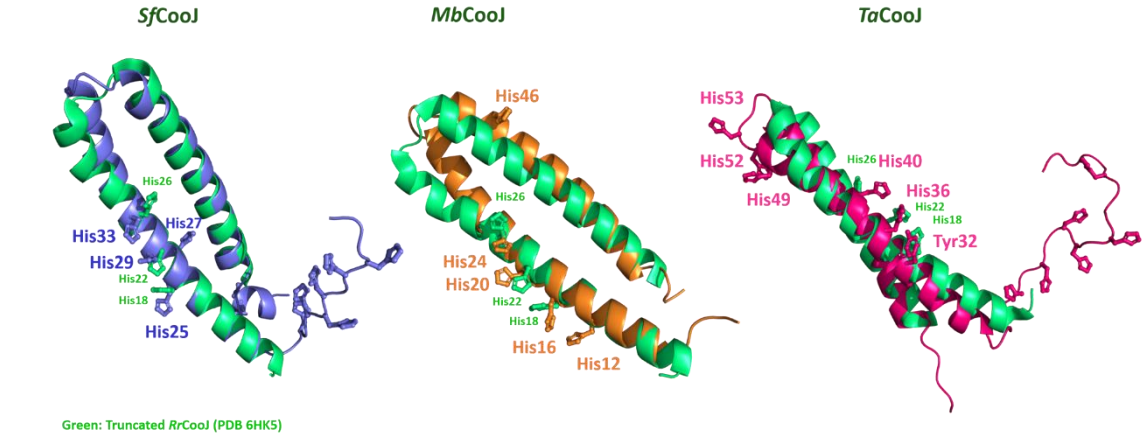
SfCooJ
MbCooJ
TaCooJ
His26
His27
His33
His29
His22
His18
His25
His46
His26
His24
His20
His22
His18
His16
His12
His53
His52
His49
His26
His40
His36
His22
His18
Tyr32
Green: Truncated RrCooJ (PDB 6HK5)

Figure 4

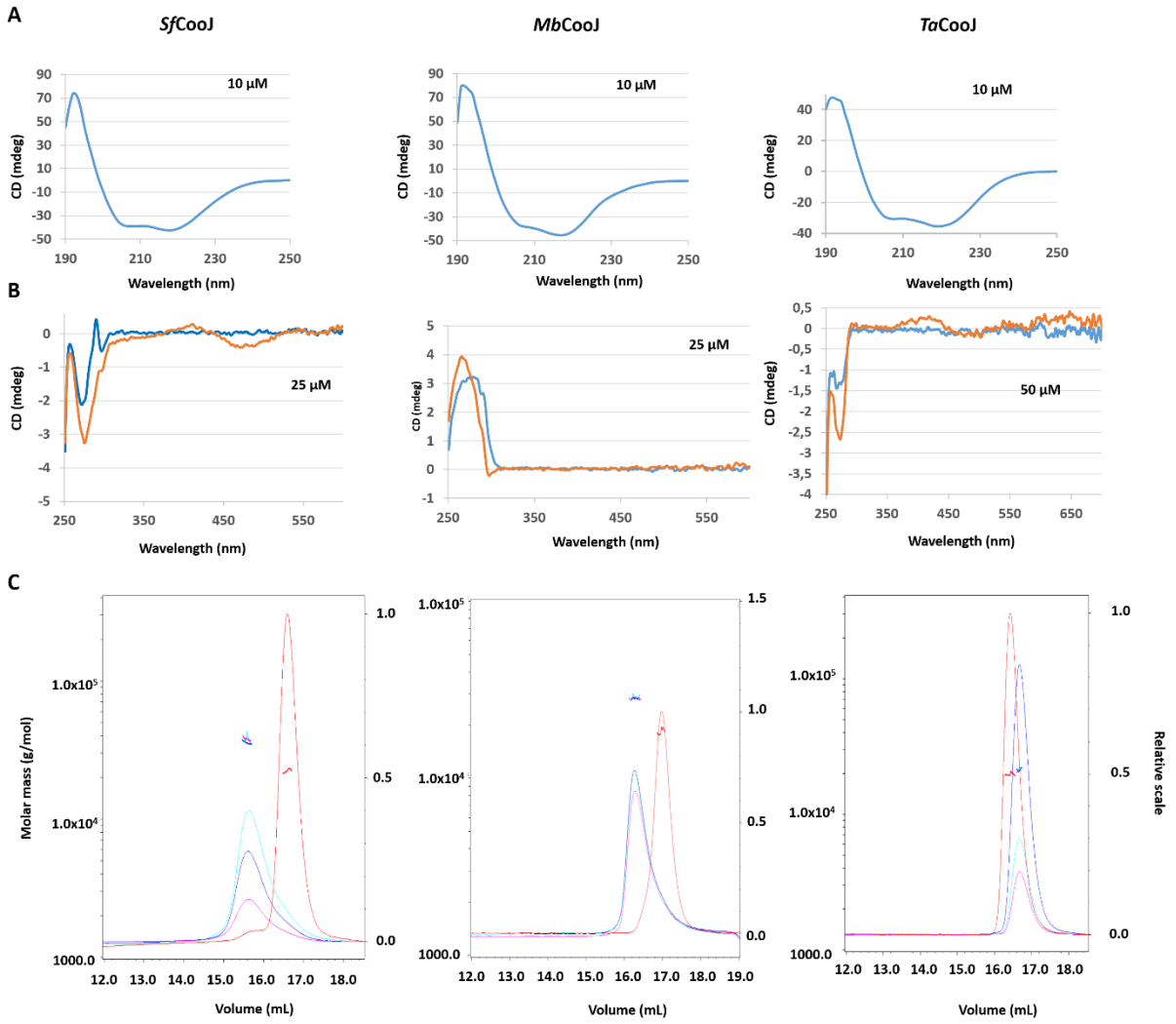
A
SfCooJ
MbCooJ
TaCooJ
10 µM
CD (mdeg)
Wavelength (nm)
B
25 µM
50 µM
C
Molar mass (g/mol)
Relative scale
Volume (mL)

Figure 5